Nuclear Instruments and Methods in Physics Research B 267 (2009) 3017–3021

Contents lists available at ScienceDirect

Nuclear Instruments and Methods in Physics Research B

journal homepage: www.elsevier.com/locate/nimb

Radiation damage evolution in ceramics

Ram Devanathan *

Chemical and Materials Sciences Division, MS K8-87, Pacific Northwest National Laboratory, Richland, WA 99352, USA

ARTICLE INFO

Article history:
Available online 14 June 2009

PACS:
02.70.−c
81.05.Je
61.80.−x
61.80.Az
61.82.Ms

Keywords:
Ceramics
Radiation damage
Radiation tolerance
Defects
Amorphization

ABSTRACT

A review is presented of recent results on radiation damage production, defect accumulation and dynamic annealing in a number of ceramics, such as silicon carbide, zircon and zirconia. Under energetic particle irradiation, ceramics can undergo amorphization by the accumulation of point defects and defect clusters (silicon carbide) or direct impact amorphization (zircon). Ceramics that resist radiation-induced amorphization have mechanisms to dissipate the primary knock-on atom energy, such as replacement collision sequences that leave the lattice undisturbed and low-energy cation site exchange. The presence of engineered mobile defects, such as structural vacancies in stabilized zirconia, can dynamically anneal radiation damage. Thus, defect engineering is a promising strategy to design radiation tolerance for applications such as nuclear waste disposal.

1. Introduction

Radiation tolerant ceramics are needed to advance nuclear energy to meet rising global energy demand and address concerns about greenhouse gas emissions. The development of novel ceramics for applications in advanced reactors and nuclear waste immobilization requires a fundamental understanding of defect production, accumulation and annealing in irradiated ceramics. Moreover, the study of the response of ceramics to non-equilibrium concentration of defects created by energetic recoils can provide insights into the rich defect chemistry of ceramics that is relevant to other applications, such as solid-oxide fuel cells and energy storage.

Several recent articles have discussed the radiation response of ceramics [1–5]. The aim of this review is to highlight recent findings from computer simulation of radiation-induced defects in ceramics. Due to the breadth of this field, this review does not aim to be comprehensive. The objective is to present results from recent simulations of defects in ceramics, such as silicon carbide, zircon and zirconia, and draw conclusions about the radiation stability of ceramics. Promising areas for further exploration are also identified.

2. Defect production and accumulation in ceramics

Radiation damage can result in amorphization of ceramics by the gradual accumulation of defects or by direct impact in the displacement cascade. Amorphization is undesirable in a material for nuclear applications as it is often accompanied by degradation of thermo-mechanical properties and reduced chemical durability. In this section, we will review radiation-induced amorphization in a ceramic that is amorphized by defect accumulation and one that undergoes direct impact amorphization.

2.1. Silicon carbide

Recent experimental ([6–8] and references therein) and simulation studies [9–12] have examined defect production by energetic electrons and recoils and the accumulation of radiation damage in silicon carbide (SiC). Molecular dynamics (MD) simulations of Si and Au recoils with energies up to 50 keV [9] in SiC have shown that the primary damage state consists of vacancies, interstitials, anti-site defects and nanoscale defect clusters. The occurrence of anti-sites in the recoil damage is interesting in light of a modeling study that concluded that short-range chemical disorder, represented by the C–C homonuclear bond ratio (χ), contributes to amorphization in SiC [10]. A subsequent MD simulation study of the overlap of 10 keV Si displacement cascades showed the average energy per atom increasing linearly with χ and eventually resulting in amorphization [11].

* Tel.: +1 509 371 6487; fax: +1 509 371 6242.
E-mail address: ram.devanathan@pnl.gov

0168-583X/$ - see front matter © 2009 Elsevier B.V. All rights reserved.
doi:10.1016/j.nimb.2009.06.020

C–C homonuclear bonds have been experimentally-observed in SiC irradiated with 200 keV electrons [6]. These authors attributed the eventual amorphization of SiC by 200 keV electron irradiation to displacements predominantly on the C sublattice giving rise to C interstitials. Our previous MD simulations [12] provided an interpretation of the above experiment by demonstrating that cubic SiC (3C polytype) can be amorphized exclusively by carbon displacements at a displacement dose of 0.2 displacements per atom (dpa) with a decrease in density of about 15%. Just below the dose for amorphization, the damage consisted predominantly of C Frenkel pairs (68%), while Si Frenkel pairs and anti-site defects made up about 14–18% each. The Si Frenkel pairs and anti-site defects were self-generated above a critical C Frenkel pair concentration. The variation of χ with dose was similar to the variation of enthalpy with dose as observed in a previous simulation of cascade overlap [11].

Recently, we have used molecular dynamics simulations with a Brenner-type potential [13] to study the effect of Si sublattice displacements on the phase stability of 3C–SiC. The simulations were performed in the isothermal isobaric ensemble at 100 K and zero external pressure. Starting with a simulation cell containing $8 \times 8 \times 8$ unit cells (496 atoms), equilibrated for 40 ps, we displaced randomly chosen Si atoms by 3.5 Å. The cell was allowed to relax for 0.2 ps between displacements. Fig. 1(a) shows the change in enthalpy (H) and χ with displacement dose. SiC is completely amorphized (based on evidence from the radial distribution function (RDF)) at a dose of 0.15 dpa, shown by the arrow, compared to 0.2 dpa for C displacements. The changes in H and χ with dose are quite similar. The dashed and dashed-dotted lines indicate the values of H and χ, respectively, for a reference amorphous state produced by quenching from the melt at 6000–50 K at the rate of 10^{14} K/s and relaxing the system at 100 K for 20 ps.

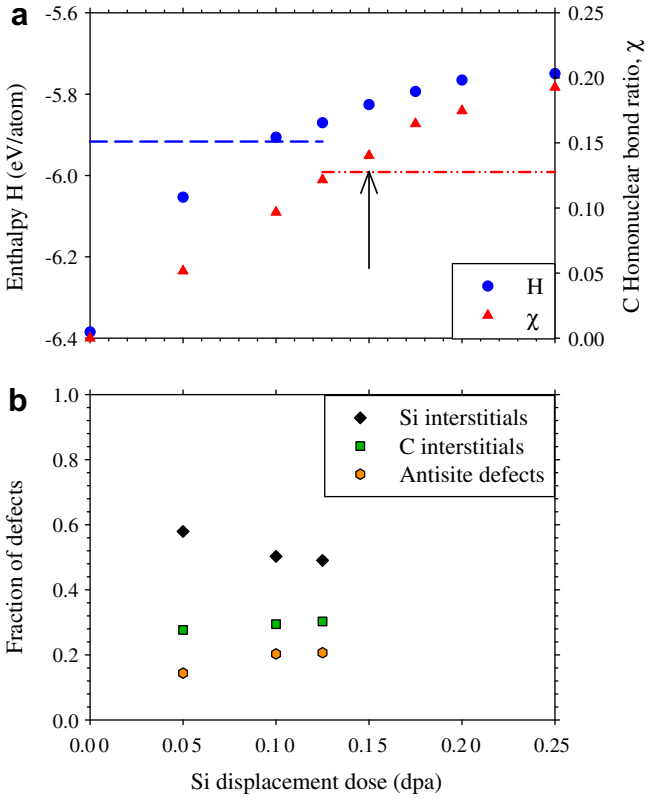

Fig. 1. The variation of (a) enthalpy (circle) and C homonuclear bond ratio (triangle) and (b) fractions of various defects with Si displacement dose.

Fig. 1(b) shows the change in relative proportions of various defects with increasing dose. The fraction of defects is shown only for doses below the amorphization dose. Once the material becomes amorphous, our criterion based on occupation of Voronoi polyhedra centered on lattice sites cannot be used to identify defects. Si Frenkel pairs are the dominant defects and the amorphization is accompanied by a density decrease of about 13%, which is slightly less than the 15% density decrease for amorphization by C displacements. It is clear that the accumulation of short-range chemical disorder, measured by χ, is a fundamental mechanism underlying amorphization regardless of the sublattice in which displacement is created and the relative proportions of various defects.

The occurrence of amorphization at a critical level of displacement or volume expansion regardless of how it is produced is consistent with the generalized Lindemann criterion for melting and amorphization that has been applied previously to metallic materials [14,15] and oxides [16]. The amorphous states of SiC produced by melt quenching, C displacement and Si displacement appear to be slightly different based on the values of χ and density, although the difference was not clearly evident from the RDF. This shows that amorphous SiC can exist in states with slightly different densities, and the RDF is not a sensitive measure of topological disorder.

2.2. Zircon

Zircon ($ZrSiO_4$) is a durable mineral that has been proposed as a candidate waste form for immobilization of high-level nuclear waste. Radiation-induced structural changes can result in enhanced leaching of cations that has significant implications for the use of zircon not only in nuclear waste disposition but also in geochronology. Previous experimental studies were ambiguous on whether radiation-induced amorphization occurs mainly by direct impact amorphization or by overlap of multiple disordered regions [17]. In an effort to examine the nature of amorphization of zircon and study the primary damage state, we have performed MD simulations of 30 keV U recoils at 300 K in the microcanonical ensemble using the DL_POLY code [18]. Zircon was modeled using a partial charge model with Buckingham-type potentials joined smoothly to a repulsive potential at short distances as discussed elsewhere [19]. The simulation cell consisted of $35 \times 35 \times 38$ unit cells. A variable time step (0.01–1 fs) algorithm was used to achieve computational efficiency with good energy conservation.

Fig. 2 is a plot of the total number of atoms displaced (N_d) more than 2 Å from their lattice sites in two cascades initiated by 30 keV U recoils along the <0 0 1> direction in zircon. This energy is

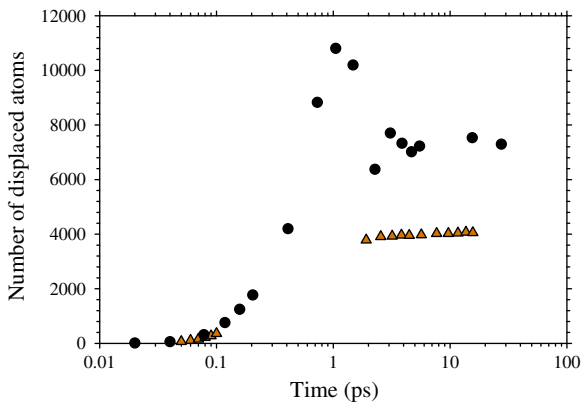

Fig. 2. The evolution of the number of displaced atoms in cascades produced by 30 keV U recoils in $ZrSiO_4$ along [0 0 1] (triangle) and [0 0 $\bar{1}$] (circle).

comparable to the damage energy of a Th recoil in natural zircon. The steady state values of N_d are about 4050 and 7300 atoms, respectively, for recoils along [0 0 1] and [0 0 $\bar{1}$]. Due to the computational intensity of these simulations in systems with long-range Coulombic interactions, we were unable to simulate more cascades to get good statistics at this high energy. However, we have previously performed MD simulations of 180 recoils (U, Zr, Si or O) with energy between 0.25 and 5 keV along 10 randomly chosen directions (usually low-symmetry directions) [20]. The choice of crystallographic directions did not affect the conclusions of the study. Defect production, mixing in the cascade and Si-polymerization increased, while the scatter in the data decreased with increasing PKA mass as well as increasing PKA energy [20].

For 30 keV U recoils, about 30% of the displacements were cations and Si displacements constituted 15–17% of N_d. A recent nuclear magnetic resonance (NMR) study of natural zircon estimated that about 5000 permanently displaced atoms are produced per α recoil by assuming that N_d is six times the number of Si displacements [21]. Our MD simulations are consistent with this experimental estimate of N_d and justify using the stoichiometric ratio in zircon to estimate this value from Si displacements.

One cannot directly estimate the number of defects produced in MD simulations from N_d, because displaced atoms may end up at equivalent sites (replacements) without creating defects. Moreover, a highly disordered region can be created by displacing a number of adjacent atoms by a distance less than 2 Å each. Fig. 3 shows a 115 Å × 70 Å projection of atoms along [1 0 0] at about 27 ps after initiation of a 30 keV U recoil along [0 0 $\bar{1}$] at 300 K. Dense damage accumulation and apparent in-cascade amorphization is evident. The defect identification algorithm based on Voronoi polyhedra employed to detect the mostly isolated defects in SiC is unsuitable for characterizing the dense damage in zircon. Previous MD simulations [22,23] have shown that energetic recoil damage results in Si–O–Si polymerization and under-coordination of Zr. We have developed algorithms for identifying defects and amorphous regions based on these characteristics of radiation damage in zircon [24].

We determined that 30 keV U recoils in zircon produce 5250–6550 defects with about 25% being Zr defects, 16–20% being Si defects and the rest O defects. About 37–50% of defects were estimated to be "amorphous atoms" based on the criterion that a majority of their neighbors were also defects. The high proportion of amorphous atoms in the primary damage state supports amorphization of zircon by direct impact in the cascade. The proportion of Zr, Si and O in the amorphous regions was about 19–20%, 21–24% and 57–59%, respectively. This indicates the formation of an amorphous core that is relatively enriched in Si surrounded by a defect region that is enriched in Zr.

The general features of the 30 keV U recoil damage along high-symmetry directions discussed above have also been observed in cascades produced by 5 keV U, Zr, Si and O recoils along low-symmetry directions [20]. In particular, nanoscale chemical segregation that is evident from Fig. 3 may provide a fundamental mechanism for the experimentally-observed phase separation of $ZrSiO_4$ into amorphous SiO_2 and nanocrystalline ZrO_2 upon irradiation at elevated temperature [25]. In addition to the damage region discussed above, small amorphous clusters that are well separated from each other and from the main amorphous core are produced due to ions travelling away from the damage core region in the form of replacement collision sequences. In ceramics that undergo in-cascade amorphization, radiation damage cannot be realistically modeled by Frenkel pair accumulation, because the distribution of defect clusters and amorphous regions, chemical segregation and the formation of regions of varying density in the cascade [22,23] will not be reproduced.

3. Dynamic defect recovery in ceramics

The radiation response of materials is governed by a dynamic balance between damage build up by defect accumulation or direct impact amorphization and dynamic annealing in the cascade as well as thermal defect recovery. The cases of SiC and $ZrSiO_4$ discussed in the preceding section represent the dominance of defect accumulation over recovery. The present section will discuss cases where defect recovery is dominant with the aim of understanding mechanisms governing radiation tolerance of ceramics.

Recently, we performed MD simulations of 30 keV Zr recoils along [0 0 1], [1 1 0] and [1 1 1] directions in zirconia and 10 mole% yttria-stabilized zirconia (YSZ) at 300 K using a formal charge model with Buckingham-type potentials. The details of the simulations and the interatomic potentials can be found elsewhere [26]. These ceramics are known to resist radiation-induced amorphization even after irradiation to hundreds of dpa [27]. Fig. 4 shows the evolution of the number of 'hot' atoms with kinetic energy in excess of 1 eV, N_d and number of interstitials in YSZ. The data from recoils along three high-symmetry directions are quite similar.

The number of hot atoms increases with time up to 0.1 ps as energy is transferred from the primary knock-on to secondary

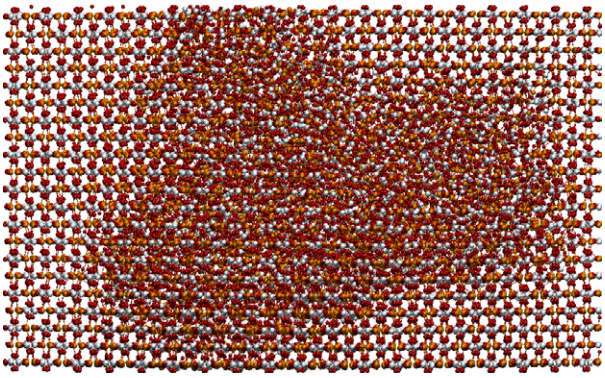

Fig. 3. Atomic projection (115 × 70 Å) showing the primary damage state of zircon after a 30 keV U recoil along [0 0 $\bar{1}$]. The initial velocity of the recoil is along the horizontal direction from right to left. Zr, Si and O atoms are represented as orange (dark gray), light gray and red (black) spheres, respectively. (For interpretation of the references to colour in this figure legend, the reader is referred to the web version of this article.)

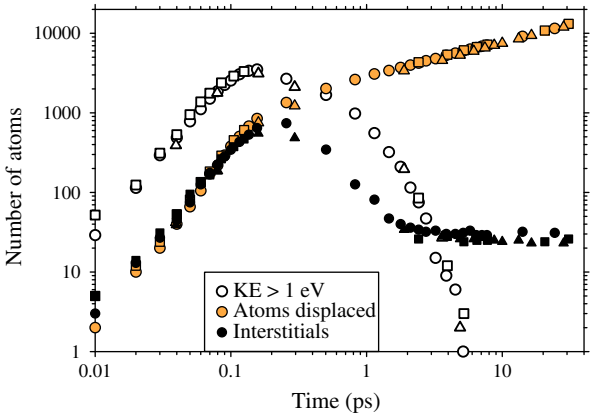

Fig. 4. The number of atoms with kinetic energy in excess of 1 eV (open symbols), atoms displaced (N_d) more than 2 Å from their lattice sites (orange/gray) and interstitials (black) from 30 keV Zr recoils in yttria-stabilized zirconia. Circles, squares and triangles represent [0 0 1], [1 1 0] and [1 1 1] recoils, respectively. (For interpretation of the references to colour in this figure legend, the reader is referred to the web version of this article.)

knock-on atoms. During this stage, N_d and the number of interstitials are nearly the same. Around 0.2–0.5 ps, the number of cation displacements reaches a steady value, but the number of anion displacements continues to increase leading to an increase in N_d with time and a change in slope of the N_d curve. The number of interstitials decreases drastically. These changes are due to the high mobility of oxygen structural vacancies that are present in YSZ for charge compensation when Y^{3+} is substituted for Zr^{4+}. The doping level of 10 mole% Y_2O_3 corresponds to 4.5% of the O sites being vacant. Most of these vacancies are located within a distance of 4 Å from anion interstitials created by 30 keV Zr recoils. In addition, barriers for O migration by the vacancy mechanism in YSZ have been estimated to be as low as 0.2 eV by density functional theory calculations [28]. As a result, anion interstitials produced by the recoil effectively annihilate at structural vacancies, which in turn contributes to dynamic annealing on the cation sublattice due to strong ionic interaction.

The primary damage state in YSZ from three 30 keV Zr cascades had an average of 0.67 anion interstitials and 26 cation Frenkel pairs. The cation vacancies and interstitials are well separated from each other as shown in Fig. 5 following a recoil along [1 1 1]. For ease of visualization of defects distributed sparsely over a large region, the defects are depicted in disproportionately large sizes. In fact, some defects that are created further away from this central damage region by replacement collision sequences are not shown. Y^{3+} is preferentially displaced compared to Zr^{4+}. While Y^{3+} constituted only 18.2% of the cations, Y interstitials make up 43–44% of cation interstitials in all three cascades. Effective in-cascade annealing of radiation damage by freely-migrating O structural vacancies results in production of a few isolated defects on the cation sublattice. These could annihilate with defects produced by subsequent recoils. Our MD simulations provide an explanation for the remarkable radiation-induced amorphization-resistance of YSZ and highlight the potential of engineering radiation tolerance by defect design.

Systematic studies of defect product along multiple low-symmetry directions have not been carried out in YSZ in contrast to the case of zircon [20,22,23]. Since the damage state in YSZ is dominated by effective recombination of isolated defects produced near structural vacancies, a change in the direction of the primary knock-on atom is unlikely to change the general conclusions regarding defect recovery.

It is also worth mentioning that the recoil energy in YSZ is dissipated mainly by creating replacement collisions on the oxygen sublattice that do not create defects. Similar mechanisms of dissipating the incident energy are operational in other ceramics. For instance, magnesium aluminate spinel ($MgAl_2O_4$) is known to resist radiation-induced amorphization and void swelling, partly because of the ability to undergo cation disorder without a substantial energy penalty [29]. Recently, it has been argued that ceramics with a natural tendency to accommodate lattice disorder show improved amorphization-resistance [5]. A combination of low activation energy for defect recovery combined with a low-energy penalty for local disorder has been proposed as a contributor to enhanced resistance to amorphization [30]. Simulations of defect production and annealing dynamics in ceramics, such as pyrochlores that show widely different radiation response with change in chemistry, are needed in addition to the existing body of data from static calculations [5,28] to improve our understanding of radiation tolerance of complex ceramics.

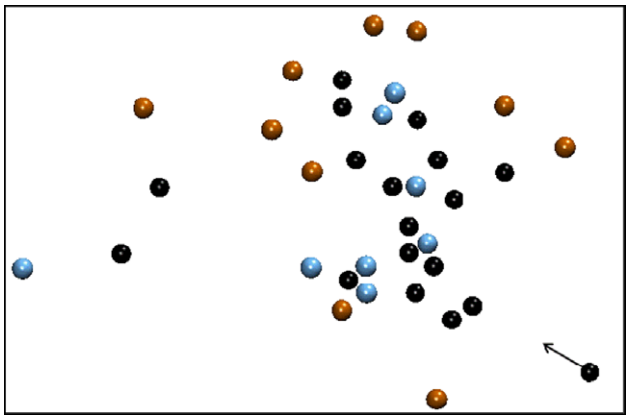

Fig. 5. Atomic projection (110 × 70 Å) showing the defects in YSZ at 28 ps after a 30 keV Zr recoil along [1 1 1]. The arrow shows the initial position and direction of the primary knock-on atom. Zr (orange/dark gray) and Y (blue/light gray) interstitials and cation vacancies (black) are shown. There were no anion interstitials. (For interpretation of the references to colour in this figure legend, the reader is referred to the web version of this article.)

4. Topics for further exploration

Most of the radiation damage simulations in ceramics to date have focused on nuclear stopping. However, electronic energy loss effects can be significant in ceramics and need to be explored. Dual-beam irradiations of α-Al_2O_3, $MgTiO_3$, $FeTiO_3$ and $Ca_2La_8(SiO_4)_6O_2$ with 1 MeV Kr^+ or 1.5 MeV Xe^+ and 1 MeV electrons have shown that simultaneous electron irradiation can retard or prevent amorphization by heavy ions even at temperatures as low as 26 K [31]. In SiC, electron irradiation has been shown to enhance dynamic defect recovery [32]. Ionization-enhanced diffusion of point defects in ceramics through mechanisms such as change in charge state of defects needs to be examined by computer simulation.

Recent studies have shown that swift heavy ion irradiation (827 MeV Pb ions) of SiC at room temperature does not cause significant damage in unirradiated samples and induces epitaxial recrystallization in samples previously damaged by low-energy (700 keV I ions) irradiation [33]. This has been explained in terms of thermal spikes but the fundamental mechanisms need to be examined in detail by simulation. Swift heavy ion irradiation has also been shown to cause crystalline-to-crystalline phase transformations in irradiated ceramics, such as zirconia [34]. In $ZrSiO_4$, swift heavy ion irradiation under high pressure has been shown to result in the formation of zircon and reidite nanocrystals [35]. The combined effects of stress, temperature and ionizing radiation on microstructural evolution needs to be studied. Preliminary simulations of swift heavy ion irradiation of ceramics have modeled a thermal spike by imparting a certain kinetic energy to atoms within a nano-sized cylinder and following the structural evolution [36]. A more recent approach [37] is to include electronic stopping and electron–ion interactions in the MD equations of motion by means of a friction term. However, this has been applied mainly to metallic systems.

Another topic of great interest is the radiation response of nanostructured ceramics [38]. A recent study compared the radiation response of nanocrystalline (NC) and large-grained polycrystalline $MgGa_2O_4$ when irradiated at 100 K with 300 keV Kr^{++} ions [39]. NC $MgGa_2O_4$ remained crystalline at an ion fluence one order of magnitude higher than that needed to amorphize polycrystalline $MgGa_2O_4$. This response is in contrast to the case of 3 nm-sized ZrO_2 crystals embedded in amorphous SiO_2 that go amorphous readily upon irradiation with 1 MeV Xe ions [40], while single crystal samples of ZrO_2 resist amorphization even at damage doses that are two orders of magnitude higher [27]. Defect annihilation at interfaces and surfaces, interfacial stresses, interfacial segregation, space charge layer formation and changes in defect diffusion at interfaces, changes in relative phase stability with particle size, and influence of the surrounding matrix are some of the factors

that need to be understood in order to draw conclusions about the radiation response of nanostructured ceramics.

5. Conclusions

The radiation response of ceramics is dictated by a delicate balance between radiation damage accumulation and damage recovery due to dynamic in-cascade processes as well as thermal annealing. Damage accumulation may occur by the gradual build up of point defects and defect clusters, overlap of highly damaged regions or direct impact amorphization in the cascade. The availability of low-energy penalty mechanisms to dissipate the incident energy, such as cation site exchange and anion replacement sequences, and the presence of 'designed' freely-migrating defects that can annihilate radiation damage can enhance radiation tolerance of ceramics. Further work is needed to understand the role of electronic energy loss processes in microstructural evolution of irradiated ceramics. The radiation response of nanostructured ceramics is another subject that needs to be understood to develop novel radiation tolerant materials for nuclear applications.

Acknowledgements

This research was supported by the Division of Materials Science and Engineering, Office of Basic Energy Sciences, US Department of Energy (DOE) under Contract No. DE-AC05-76RL01830. This research was performed in part using the Molecular Science Computing Facility in the Environmental Molecular Sciences Laboratory, a national scientific user facility sponsored by the US DOE, Office of Biological and Environmental Research and located at Pacific Northwest National Laboratory (PNNL). It used resources of the National Energy Research Scientific Computing Center, which is supported by the Office of Science of the US Department of Energy under Contract No. DE-AC02-05CH11231. The author thanks William J. Weber (PNNL) for valuable discussions and insights into radiation tolerance of ceramics.

References

[1] S.J. Zinkle, C. Kinoshita, J. Nucl. Mater. 251 (1997) 200.
[2] W.J. Weber, R.C. Ewing, C.R.A. Catlow, T. Diaz de la Rubia, L.W. Hobbs, C. Kinoshita, H.J. Matzke, A.T. Motta, M. Nastasi, E.H.K. Salje, E.R. Vance, S.J. Zinkle, J. Mater. Res. 13 (1998) 1434.
[3] K. Trachenko, M.T. Dove, E. Artacho, I.T. Todorov, W. Smith, Phys. Rev. B 73 (2006) 174207.
[4] L. Thomé, A. Gentils, J. Jagielski, F. Garrido, T. Thomé, Vacuum 81 (2007) 1264.
[5] K.E. Sickafus, R.W. Grimes, J.A. Valdez, A. Cleave, M. Tang, M. Ishimaru, S.M. Corish, C.R. Stanek, B.P. Uberuaga, Nat. Mater. 6 (2007) 217.
[6] M. Ishimaru, I.-T. Bae, Y. Hirotsu, Phys. Rev. B 68 (2003) 144102.
[7] W.J. Weber, F. Gao, R. Devanathan, W. Jiang, C.M. Wang, Nucl. Instr. and Meth. B 216 (2004) 25.
[8] A. Benyagoub, Nucl. Instr. and Meth. B 266 (2008) 2766.
[9] F. Gao, W.J. Weber, J. Mater. Res. 18 (2003) 1877.
[10] X. Yuan, L.W. Hobbs, Nucl. Instr. and Meth. B 191 (2002) 74.
[11] F. Gao, W.J. Weber, Phys. Rev. B 66 (2002) 024106.
[12] R. Devanathan, F. Gao, W.J. Weber, Appl. Phys. Lett. 84 (2004) 3909.
[13] F. Gao, W.J. Weber, Nucl. Instr. and Meth. B 191 (2002) 504.
[14] N.Q. Lam, P.R. Okamoto, MRS Bull. 19 (1994) 41.
[15] R. Devanathan, N.Q. Lam, P.R. Okamoto, M. Meshii, Phys. Rev. B 48 (1993) 42.
[16] K.E. Sickafus, N. Yu, M. Nastasi, J. Nucl. Mater. 304 (2002) 237.
[17] C.S. Palenik, L. Nasdala, R.C. Ewing, Am. Mineral. 88 (2003) 770.
[18] I.T. Todorov, W. Smith, K. Trachenko, M.T. Dove, J. Mater. Chem. 16 (2006) 1911.
[19] R. Devanathan, L.R. Corrales, W.J. Weber, A. Chartier, C. Meis, Phys. Rev. B 69 (2004) 064115.
[20] R. Devanathan, L.R. Corrales, W.J. Weber, A. Chartier, C. Meis, Nucl. Instr. and Meth. B 228 (2005) 299.
[21] I. Farnan, H. Cho, W.J. Weber, Nature 445 (2007) 190.
[22] J.-P. Crocombette, D. Ghaleb, J. Nucl. Mater. 295 (2001) 167.
[23] K.O. Trachenko, M.T. Dove, E.K.H. Salje, Phys. Rev. B 65 (2002) 180102.
[24] R. Devanathan, L.R. Corrales, W.J. Weber, A. Chartier, C. Meis, Mol. Simul. 32 (2006) 1069.
[25] A. Meldrum, S.J. Zinkle, L.A. Boatner, R.C. Ewing, Nature 395 (1998) 56.
[26] R. Devanathan, W.J. Weber, J. Mater. Res. 23 (2008) 593.
[27] K.E. Sickafus, H.J. Matzke, T. Hartmann, K. Yasuda, J.A. Valdez, P. Chodak III, M. Nastasi, R.A. Verrall, J. Nucl. Mater. 274 (1999) 66.
[28] R. Pornprasertsuk, P. Ramanarayanan, C.B. Musgrave, F.B. Frinz, J. Appl. Phys. 98 (2005) 103513.
[29] K.E. Sickafus, L. Minervini, R.W. Grimes, J.A. Valdez, M. Ishimaru, F. Li, K.J. McClellan, T. Hartmann, Science 289 (2000) 748.
[30] M.J.D. Rushton, C.R. Stanek, A.R. Cleave, B.P. Uberuaga, K.E. Sickafus, R.W. Grimes, Nucl. Instr. and Meth. B 255 (2007) 151.
[31] R. Devanathan, K.E. Sickafus, W.J. Weber, M. Nastasi, J. Nucl. Mater. 253 (1998) 113.
[32] I.-T. Bae, W.J. Weber, M. Ishimaru, Y. Hirotsu, Appl. Phys. Lett. 90 (2007) 121910.
[33] A. Benyagoub, A. Audren, L. Thomé, F. Garrido, Appl. Phys. Lett. 89 (2006) 241914.
[34] A. Benyagoub, Nucl. Instr. and Meth. B 218 (2004) 451.
[35] U.A. Glasmacher, M. Lang, H. Keppler, F. Langenhorst, R. Neumann, D. Schardt, C. Trautmann, G.A. Wagner, Phys. Rev. Lett. 96 (2006) 195701.
[36] R. Devanathan, P. Durham, J. Du, L.R. Corrales, E.M. Bringa, Nucl. Instr. and Meth. B 255 (2007) 172.
[37] D.M. Duffy, A.M. Rutherford, J. Phys.: Condens. Matter 19 (2007) 016207.
[38] T.D. Shen, Nucl. Instr. and Meth. B 266 (2008) 921.
[39] T.D. Shen, S. Feng, M. Tang, J.A. Valdez, Y. Wang, K.E. Sickafus, Appl. Phys. Lett. 90 (2007) 263115.
[40] A. Meldrum, L.A. Boatner, R.C. Ewing, Phys. Rev. Lett. 88 (2002) 025503.